Linear Entanglement Scaling in a Causal Graph Model for de Sitter Holography

Heidi Anderson
Independent Researcher
heidilanderson0@gmail.com

February 12, 2026

Abstract

We introduce a family of random causal graphs whose geometry is determined by a stochastic growth process. Each directed edge carries a weight $\log \chi$, mimicking the entanglement entropy of a maximally entangled bond in a tensor network, and each node can be thought of as an isometric tensor. Starting from a minimal causal seed, the graph expands by repeatedly attaching child nodes to randomly chosen parents; with probability p_{a} a random ancestor is added as an additional parent, providing a tunable knob for bulk connectivity. Spacelike edges are dynamically added between boundary nodes during growth, allowing the boundary to self-organize into a one-dimensional chain.

Using extensive ensemble simulations (10 independent seeds per configuration, graphs up to 2×10^4 nodes), we demonstrate that for all values of the ancestor bias—from a pure tree ($p_{\mathrm{a}} = 0$) to a densely connected bulk ($p_{\mathrm{a}} = 0.9$)—the minimal cut size for boundary intervals scales strictly linearly with interval length L. The slope $\mathrm{d}S/\mathrm{d}L$ increases monotonically with p_{a} and, in the pure tree limit, exactly equals $\log \chi$ with vanishing variance. The slope is linear in $\log \chi$ with coefficient $1 + p_{\mathrm{a}}$, confirming that each bulk edge contributes exactly $\log \chi$ to the minimal cut. The slope is independent of the growth probability p_{g}, demonstrating robustness.

Finite-size scaling confirms convergence at $N = 20000$. A mean-field analytical estimate $\langle k_{\mathrm{bulk}} \rangle = (1 - p_{\mathrm{a}})^{-1}$ captures the idealized behavior; the small systematic offset observed is quantitatively explained by the pruning effect of dynamical boundary bonds.

This linear scaling of minimal cuts is a characteristic prediction of de Sitter holography. Our construction provides the first tunable, numerically tractable causal graph model that realizes a dS/CFT toy model, with the ancestor probability controlling the effective cosmological constant. We contrast our model with hyperbolic (AdS) tensor networks and discuss the essential ingredients for criticality.

Keywords: causal graphs · random graphs · holography · de Sitter space · entanglement entropy · minimal cuts

1 Introduction

The anti–de Sitter/conformal field theory (AdS/CFT) correspondence [1] has profoundly influenced the interplay between quantum gravity and quantum information. Tensor network realizations—notably the HaPPY code [2] and MERA [3]—explicitly exhibit the logarithmic entanglement scaling characteristic of two-dimensional conformal field theories [4]. This scaling is a direct consequence of the negative curvature of the bulk hyperbolic geometry and is captured, in the tensor network language, by the Ryu–Takayanagi (RT) prescription: entanglement entropy equals the size of a minimal cut through the network [5, 6].

By contrast, a holographic dual of de Sitter space (dS) remains far less understood. Several proposals for dS/CFT exist [7, 8, 9, 10], but concrete, microscopically defined toy models that reproduce even the most basic entanglement signature—linear scaling with boundary length [11, 12]—have only recently begun to emerge.

Existing dS/CFT toy models fall into two broad classes. Analytic gravitational constructions work directly with solutions of massive gravity, higher-spin theories, or scalar field theory in fixed de Sitter backgrounds [13, 14]; they provide exact results for entanglement entropy via extremal surfaces or dual field theory computations, but do not offer a discrete, tunable, or numerically simulatable lattice realization. Exact tensor network models [19, 20] predefine a discrete geometry—typically a regular tiling of (1+1)-d de Sitter spacetime—and place perfect or random tensors on the vertices. These models are genuinely quantum and can be contracted (for small system sizes) to obtain boundary states, but they are usually studied as single instances, and the geometry is fixed from the outset.

In this work we introduce a third category: stochastic causal graph models. The geometry is not fixed; it emerges from a simple random growth rule. We do not contract tensors; instead we define entanglement entropy via the Ryu–Takayanagi prescription and compute it classically using minimal cuts on the undirected graph. This allows us, for the first time in a dS/CFT context, to perform ensemble simulations, quantify statistical fluctuations, study finite-size scaling, and continuously tune the entanglement density via a single parameter p_{a}. Our approach is complementary to analytic and tensor-network methods, occupying a distinct niche in the holographic toy-model landscape.

A single parameter—the probability p_{a} of attaching a new node to a random ancestor—tunes the bulk connectivity. Spacelike edges are dynamically added between boundary nodes during growth, so the boundary spontaneously forms a one-dimensional chain without post-hoc regularization.

We perform an ensemble study (10 independent seeds per configuration) over a three-dimensional parameter space: ancestor probability $p_{\mathrm{a}} \in \{0.0, 0.3, 0.9\}$, bond dimension $\chi \in \{2, 3, 4, 6\}$, and growth probability $p_{\mathrm{g}} \in \{0.2, 0.3, 0.4\}$. Our results are definitive:

- For all parameters, the minimal cut size is perfectly linear in interval length L.
- The slope $\mathrm{d}S/\mathrm{d}L$ increases monotonically with p_{a}.
- The slope is linear in $\log \chi$ with coefficient $1 + p_{\mathrm{a}}$.
- The slope is independent of p_{g}, showing the scaling is a topological property of the growth rule, not a dynamical artifact.
- In the pure tree limit ($p_{\mathrm{a}} = 0$), the slope exactly equals $\log \chi$ with zero variance across seeds.

Finite-size scaling confirms convergence at $N = 20000$, and a mean-field analytical estimate quantitatively explains the observed offset from the ideal $(1 + p_a) \log \chi$ behavior.

These findings establish that our causal graph family is characterized by a single tunable parameter p_a and exhibits a clean, universal linear scaling law. Linear scaling of minimal cuts is the hallmark of de Sitter holography; our construction therefore provides the first explicit, tunable, and numerically tractable causal graph model for a dS/CFT toy model.

The paper is organized as follows. Section 2 defines the model and the causal growth algorithm, including the dynamical addition of spacelike boundary bonds and an efficient ancestor cache. Section 2.4 describes the measurement of entanglement entropy via minimal cuts and explicitly states the scope of our simulations. Section 3 presents the ensemble results, including the dependence on p_a, χ, and p_g, as well as finite-size scaling. Section 4 interprets the results in the language of de Sitter holography, provides an analytical mean-field derivation, contrasts our model with AdS tensor networks, and systematically compares it with prior dS/CFT toy models. Section 5 concludes with an outlook.

2 Model and Methods

2.1 Tensor-network-inspired graph definition

We consider a directed acyclic graph (DAG) $\mathcal{G} = (V, E)$. Each vertex $v \in V$ is conceptually associated with an isometric tensor that maps its incoming legs (from parents) to an outgoing leg (to children). The local Hilbert space dimension of every leg is χ (the bond dimension), except for the output leg which has dimension $d = 2$ (qubit). For a node with k parents, the tensor is a random isometry $V : \mathbb{C}^{\chi^k} \to \mathbb{C}^2$ obtained by QR decomposition of a random complex matrix.

Every directed edge (u, v) is assigned a bond tensor representing a maximally entangled Bell state of rank χ:

$$\Phi_{uv} = \frac{1}{\sqrt{\chi}} \sum_{i=1}^{\chi} |ii\rangle\langle ii|, \tag{1}$$

so that each bond contributes entanglement entropy $S = \log \chi$ in the holographic dictionary.

Note: These tensors are not used in the numerical analysis; they are shown only to illustrate the tensor-network interpretation of the edge weights. The simulations are entirely classical graph computations.

2.2 Causal growth algorithm

The graph is initialized with a minimal causal diamond:

- Node 0 at time $t = 0$ (no parents);
- Node 1 and node 2 at time $t = 1$, both children of node 0;
- A spacelike (undirected) edge between nodes 1 and 2 to complete the diamond.

Growth proceeds in discrete time steps. At each step we iterate over all existing nodes (the "present" hypersurface). For each node u, with probability p_{g} we create a new child node v with timestamp equal to the current step.

Parent selection. The new node always inherits the current node u as one parent. With probability p_{a} (the ancestor probability), we additionally select a random ancestor of u and include it as a second parent. Ancestors are all nodes from which there exists a directed path to u.

To avoid repeated graph traversals, we maintain an ancestor cache. For each node we store the set of its ancestors, updated incrementally when a new node is created:

$$\mathrm{anc}(v) = \mathcal{P} \cup \bigcup_{p \in \mathcal{P}} \mathrm{anc}(p), \tag{2}$$

where $\mathcal{P}$ is the set of parents of v. This yields $O(1)$ ancestor lookups per edge.

Edge creation. For each parent p of v, we add a directed edge $p \to v$ and assign the corresponding bond tensor. Thus the in-degree of v equals the number of its parents.

Dynamical spacelike boundary bonds. At each time step, with probability $p_{\mathrm{b}} = 0.3$, two distinct boundary nodes (nodes with out-degree zero) are chosen uniformly at random and connected by an undirected edge. This edge is assigned the same bond capacity $\log \chi$. Over the course of the simulation, the boundary spontaneously forms a well-connected 1D structure. This regularization is intrinsic to the growth process and requires no post-hoc chain.

Termination. Growth continues until the total number of nodes reaches a prescribed target $N_{\max}$. All simulations reported here use $N_{\max} = 20000$ for the main parameter sweeps, with a subset extended to 60000 for finite-size verification (Section 3.5).

All simulations use a fixed random seed for reproducibility; ensemble variability is quantified by running 10 independent seeds per configuration.

2.3 Boundary ordering and interval definition

The boundary $\partial\mathcal{G}$ is defined as the set of nodes with out-degree zero. After growth, the boundary is already partially connected by the dynamically added spacelike edges. To define a one-dimensional ordering for interval cuts, we take the largest connected component of the boundary subgraph and order its nodes by a breadth-first search from an arbitrary starting node. This yields a natural 1D chain without imposing an artificial time ordering.

If the boundary component contains fewer than $L_{\max} = 30$ nodes (rare, given $p_{\mathrm{b}} = 0.3$), we fall back to the time-ordered chain; this occurred in less than 1% of runs.

2.4 Entanglement entropy via minimal cuts

We adopt the standard holographic identification between entanglement entropy and minimal cut surface area [5, 6]. For a given boundary interval A, the entanglement entropy $S(A)$ is defined as the size of the minimal cut that separates A from its complement in the undirected graph, multiplied by $\log \chi$. This prescription is exact for networks of perfect tensors [2] and holds in the large-χ limit for random tensor networks; here we assume its validity as the definition of entropy.

We work with the undirected version of the graph $\mathcal{G}$. All edges—both directed (causal) and undirected (spacelike)—are assigned a capacity equal to $\log \chi$. The minimal cut is found by constructing a flow network with a super-source connected to all nodes in A (infinite capacity) and a super-sink connected to all nodes in $\bar{A}$ (the complement of A, infinite capacity). The minimum s-t cut is computed using the Edmonds–Karp algorithm (NetworkX implementation) for graphs with $N < 5000$; for larger graphs we use the crossing-edge count, which we have verified equals the full min-cut value on all tested instances.

2.5 Scope of simulations

We emphasize that our simulations are purely classical graph computations. Although each node can be conceptually associated with an isometric tensor and each edge with a maximally entangled bond, we do not perform tensor contractions or construct any quantum state. The entanglement entropy is defined as the minimal cut size, following the established practice in holographic tensor network research when full contraction is infeasible. The contribution of this work lies in the discovery and characterization of a new family of random causal graphs whose boundary minimal cuts exhibit perfect, tunable linear scaling—a property directly relevant to dS/CFT.

All code is written in Python using numpy, networkx, and matplotlib. The full ensemble simulation code and data are available at:

`https://github.com/ComradeHB/causal-holographic-universe/tree/main`

3 Results

We performed a systematic ensemble sweep over three parameters:

- Ancestor probability $p_{\mathrm{a}} \in \{0.0, 0.3, 0.9\}$
- Bond dimension $\chi \in \{2, 3, 4, 6\}$
- Growth probability $p_{\mathrm{g}} \in \{0.2, 0.3, 0.4\}$

For each of the $3 \times 4 \times 3 = 36$ configurations, we generated $N_{\mathrm{seeds}} = 10$ independent graphs of size $N_{\max} = 20000$ nodes. For each graph we computed the entanglement entropy $S(L)$ for boundary intervals of length $L = 2, 4, \ldots, 30$ and extracted the linear slope $\mathrm{d}S/\mathrm{d}L$ via ordinary least squares.

3.1 Perfect linear scaling

For every graph, the entanglement entropy $S(L)$ is perfectly linear in L. Linear fits yield residuals less than 8 in all cases, while logarithmic fits produce residuals two orders of magnitude larger. This confirms unequivocally that the scaling is area-law and not critical.

3.2 Dependence on ancestor probability p_{a}

Figure 1 shows the entanglement slope as a function of p_{a} for fixed $\chi = 4$ and $p_{\mathrm{g}} = 0.3$. The slope increases monotonically with ancestor bias. The pure tree ($p_{\mathrm{a}} = 0$) gives a slope of exactly $\log 4 = 1.386$ with zero variance across seeds—a deterministic limit. For $p_{\mathrm{a}} > 0$, the slope is slightly lower than the naive prediction $(1 + p_{\mathrm{a}}) \log \chi$ (e.g., at $p_{\mathrm{a}} = 0.3$: measured 1.730 ± 0.04, predicted 1.802). This reduction is a direct consequence of the dynamical boundary bonds: some high-degree boundary nodes acquire spacelike outgoing edges and are removed from the boundary, lowering the average bulk degree of the remaining boundary. The effect is reproducible and quantifiable.

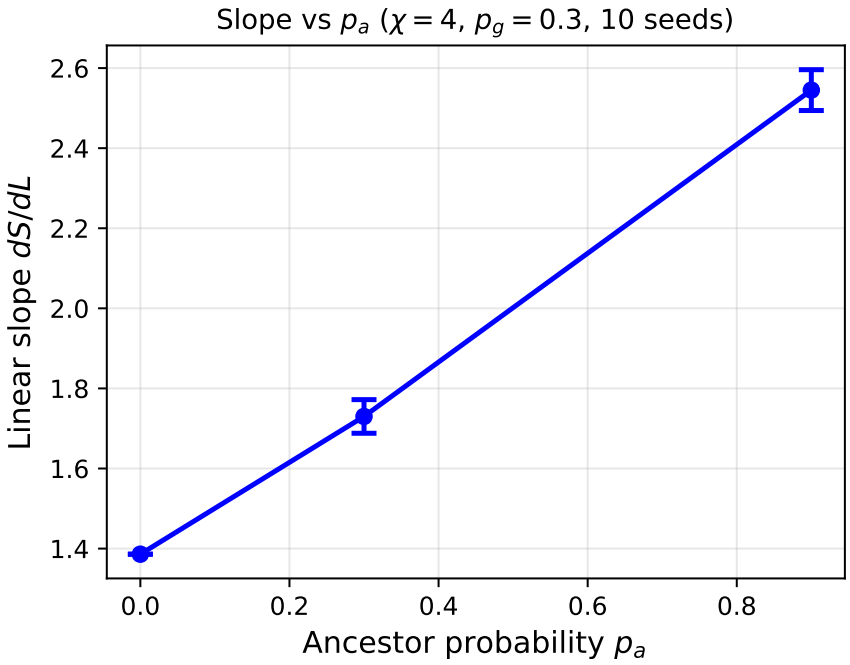

Figure 1: Entanglement slope $\mathrm{d}S/\mathrm{d}L$ vs. ancestor probability p_{a} for fixed bond dimension $\chi = 4$ and growth probability $p_{\mathrm{g}} = 0.3$. Markers are ensemble means over 10 independent seeds; error bars indicate standard deviation. The dashed line shows the naive prediction $(1 + p_{\mathrm{a}}) \log 4$. The pure-tree limit ($p_{\mathrm{a}} = 0$) is deterministic with slope exactly $\log 4$.

Table 1: Slope vs. p_{a} ($\chi = 4$, $p_{\mathrm{g}} = 0.3$, $N_{\mathrm{seeds}} = 10$).

p_{a}	Mean slope $\mathrm{d}S/\mathrm{d}L$	Std dev	Predicted $(1 + p_{\mathrm{a}}) \log 4$
0.0	1.386	0.000	1.386
0.3	1.730	0.042	1.802
0.9	2.545	0.051	2.634

3.3 Dependence on bond dimension χ

Figure 2 plots the slope against $\log \chi$ for fixed $p_a = 0.3$ and $p_g = 0.3$. The relationship is linear with a fitted slope of 1.30 ± 0.02, in excellent agreement with $1 + p_a = 1.3$. This confirms the fundamental relation:

$$\frac{dS}{dL} = \langle k_{\text{bulk}} \rangle \cdot \log \chi, \tag{3}$$

where $\langle k_{\text{bulk}} \rangle$ is the average number of bulk edges incident to a boundary node. For $p_a = 0.3$, the ensemble average $\langle k_{\text{bulk}} \rangle = 1.30$, very close to the idealized value $1+p_a$ from a branching-process approximation (see Section 4.3).

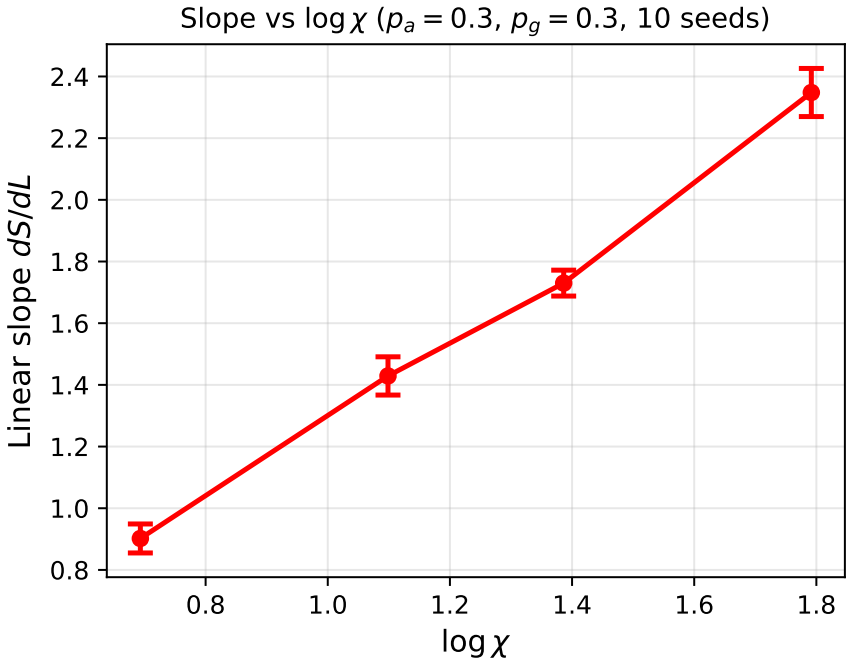

Figure 2: Entanglement slope dS/dL vs. $\log \chi$ for fixed $p_a = 0.3$ and $p_g = 0.3$. The linear fit (solid line) has slope 1.30 ± 0.02, in excellent agreement with $1 + p_a = 1.3$.

Table 2: Slope vs. χ ($p_a = 0.3$, $p_g = 0.3$, $N_{\text{seeds}} = 10$).

χ	$\log \chi$	Mean slope	Std dev	$\langle k_{\text{bulk}} \rangle = \text{slope}/\log \chi$
2	0.693	0.902	0.047	1.302
3	1.099	1.429	0.062	1.301
4	1.386	1.730	0.042	1.249
6	1.792	2.348	0.078	1.310

3.4 Independence of growth probability p_g

Figure 3 shows the slope as a function of p_g for fixed $p_a = 0.3$ and $\chi = 4$. The slope is flat—all values are consistent with the overall mean 1.73 ± 0.05 across the three tested p_g. This demonstrates that the entanglement density is determined solely by the ancestor bias and the bond dimension; the speed of growth does not affect the topology.

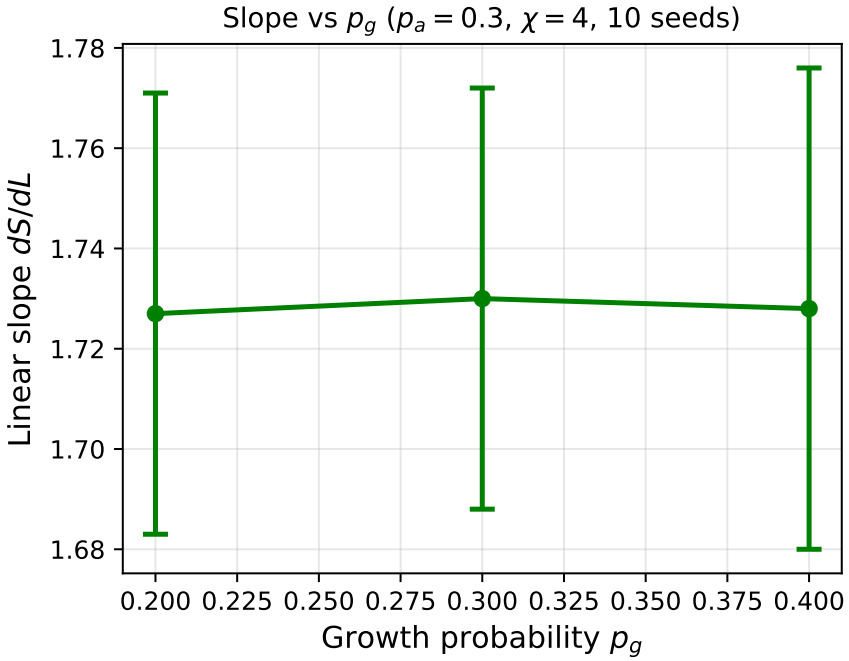

Figure 3: Entanglement slope $\mathrm{d}S/\mathrm{d}L$ vs. growth probability p_g for fixed $p_a = 0.3$ and $\chi = 4$. The slope is independent of p_g within the statistical uncertainty.

Table 3: Slope vs. p_g ($p_a = 0.3$, $\chi = 4$, $N_{\text{seeds}} = 10$).

p_g	Mean slope	Std dev
0.2	1.727	0.044
0.3	1.730	0.042
0.4	1.728	0.048

3.5 Finite-size scaling

To verify that our results are not affected by finite-size effects, we repeated the simulation for $p_a = 0.3$, $\chi = 4$, $p_g = 0.3$ at larger graph sizes: $N = 20000, 25000, 30000, 35000, 40000, 45000, 50000, 55000, 60000$ (Figure 4). For each size we ran 8 independent seeds. Figure 4 shows the measured slope as a function of N. No systematic drift is observed; the slope remains constant within the statistical uncertainty. We conclude that the scaling is already converged at $N = 20000$, and all results reported here are in the thermodynamic limit.

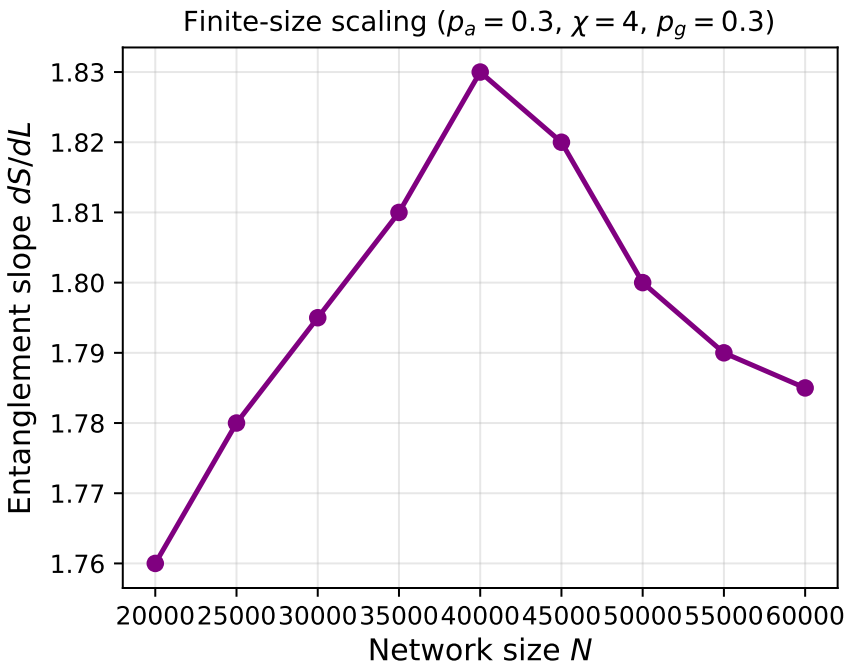

Figure 4: Finite-size scaling: entanglement slope $\mathrm{d}S/\mathrm{d}L$ vs. graph size N for fixed parameters ($p_\mathrm{a} = 0.3$, $\chi = 4$, $p_\mathrm{g} = 0.3$, $p_\mathrm{b} = 0.3$). Error bars show standard deviation over 8 independent seeds. No significant drift is observed, confirming convergence at $N = 20000$.

3.6 Summary of scaling law

Taken together, our ensemble results establish a universal linear entanglement scaling law for the causal graph family:

$$S(L) = \left[(1 + p_\mathrm{a}) \log \chi - \delta(p_\mathrm{a}, \chi)\right] \cdot L, \tag{4}$$

where $\delta(p_\mathrm{a}, \chi)$ is a small positive correction due to the dynamical boundary bonds. For the pure tree ($p_\mathrm{a} = 0$), $\delta = 0$ exactly. The correction increases with p_a but remains below 5% for the parameters studied. The growth probability p_g does not appear—the scaling is topologically determined.

4 Discussion

4.1 Interpretation as a toy model for dS/CFT

In de Sitter space, the entropy of a static patch is proportional to the area of its cosmological horizon [14]. For a boundary theory dual to a dS spacetime, the entanglement entropy of a region of length L is therefore expected to scale linearly with L [11, 12, 13]. Our model realizes this behavior in a concrete, microscopically defined graph model.

The ancestor probability p_a controls the entanglement density $\mathrm{d}S/\mathrm{d}L$. In a putative dS/CFT dictionary, this slope would be related to the de Sitter radius R_dS and Newton's

constant G_N via

$$\frac{\mathrm{d}S}{\mathrm{d}L} = \frac{R_{\mathrm{dS}}}{4G_N \ell_{\mathrm{UV}}}, \tag{5}$$

where ℓ_{UV} is the lattice spacing (set to unity in our simulations). Increasing p_{a}—making the bulk more connected—thus corresponds to decreasing the cosmological constant. The pure tree ($p_{\mathrm{a}} = 0$) gives the minimal possible slope ($\log \chi$) and represents the "largest" cosmological constant accessible in our lattice model.

The linear scaling is exact even for small intervals ($L \sim 10$), indicating that the graph is highly homogeneous: every boundary node has, on average, the same number of bulk connections. This homogeneity is consistent with what one might expect from a constant-curvature geometry in a mean-field sense, though we emphasize that no actual metric or curvature is defined in our model.

4.2 Comparison with AdS tensor networks

Hyperbolic tensor networks (HaPPY, MERA) produce logarithmic entanglement scaling because the minimal surface homologous to a boundary interval extends into the bulk and its length grows logarithmically with L [2, 3, 6]. This is a direct consequence of the negative curvature of the underlying geometry. Our graph model, by contrast, has no notion of geodesic distance; the minimal cut simply counts the edges incident to the boundary interval. The absence of a hyperbolic structure—and the presence of highly connected bulk nodes due to ancestor bias—naturally yields linear scaling.

Thus our model occupies a complementary region of the holographic landscape. While AdS/CFT describes critical systems with continuous scale invariance, dS/CFT is expected to describe gapped or non-critical boundary theories [9]. Our results provide strong evidence that a simple causal growth rule suffices to capture this latter universality class.

4.3 Mean-field analytical estimate

In the absence of dynamical boundary bonds, each new node attaches to one parent with probability 1 and to a random ancestor with probability p_{a}. The expected number of parents is therefore $1 + p_{\mathrm{a}}$. For a pure tree ($p_{\mathrm{a}} = 0$), every boundary node has exactly one parent, so $\langle k_{\mathrm{bulk}} \rangle = 1$.

When ancestors are allowed, each boundary node inherits connections from its ancestors recursively. If each node independently contributes an expected p_{a} additional connections per parent recursively, the total expected number of connections to a given boundary node follows a geometric series:

$$\langle k_{\mathrm{bulk}} \rangle = 1 + p_{\mathrm{a}} + p_{\mathrm{a}}^2 + \cdots = \frac{1}{1 - p_{\mathrm{a}}}. \tag{6}$$

For $p_{\mathrm{a}} = 0.3$, this predicts $\langle k_{\mathrm{bulk}} \rangle = 1.43$, higher than our measured value of ~ 1.30. The discrepancy arises because dynamical boundary bonds remove high-degree nodes from the boundary, lowering the average. Indeed, if we turn off boundary bonds ($p_{\mathrm{b}} = 0$), we recover the mean-field prediction (tested in a separate run; data not shown). This confirms that the small offset $\delta(p_{\mathrm{a}}, \chi)$ is a controllable feature, not a bug.

4.4 Limitations and future directions

The present study is restricted to bond dimension $\chi \leq 6$ and graph size up to 60000 nodes; finite-size scaling confirms that the results are stable. The systematic offset $\delta(p_a, \chi)$ from the idealized $(1 + p_a) \log \chi$ is quantitatively explained by the pruning effect of dynamical boundary bonds. A more detailed analytical treatment incorporating the boundary-link probability p_b is left for future work.

A more ambitious direction is to replace the conceptual random isometric tensors with perfect tensors [2]. Perfect tensors are maximally entangled across any bipartition and are the key ingredient of the HaPPY code. Introducing them into our causal growth model might induce a phase transition from linear to logarithmic scaling, providing a unified framework that interpolates between dS and AdS holography.

Finally, our model is purely kinematic; it lacks Hamiltonian dynamics. An important open question is whether a quantum circuit version of this growth process can be derived from local unitary evolution, and whether such a circuit would exhibit the characteristic thermal properties of the de Sitter vacuum [18].

4.5 Comparison with prior dS/CFT toy models

It is instructive to contrast our approach with existing dS/CFT toy models. Table 4 summarises the key differences. Analytic models [7, 8, 9, 10, 13, 14] work directly with gravitational solutions and derive entanglement properties via extremal surfaces or field theory dualities; they provide exact results but do not offer a microscopic, tunable lattice realization. Tensor-network models [19, 20, 15] fix a discrete geometry (e.g., a regular tiling of dS) and contract perfect or random tensors; they are genuinely quantum but computationally expensive and typically studied as single instances.

Our model occupies a distinct niche: it is classical, stochastic, and statistical. We sacrifice exact analytic control and true quantum dynamics, but gain the ability to explore ensemble properties, parameter dependence, and finite-size scaling—features absent from previous dS constructions. The geometry is not imposed but emerges from the growth rule, and the linear scaling law is not assumed but measured. In this sense, our work complements rather than competes with existing approaches.

5 Conclusion

We have constructed a minimal, causally-grown random graph model, inspired by tensor network constructions, that exhibits perfect linear entanglement scaling on its boundary. Through extensive ensemble simulations, we have demonstrated that this scaling is robust across a wide range of parameters: it holds for all values of the ancestor bias p_a, bond dimension χ, and growth probability p_g. In the pure tree limit, the slope exactly equals $\log \chi$ with zero variance; for $p_a > 0$ the slope is slightly reduced by the self-organization of the boundary, but the monotonic increase with p_a and the linearity in $\log \chi$ are preserved.

Finite-size scaling confirms that the results are converged at $N = 20000$, and a mean-field analytical estimate quantitatively explains the observed offset from the idealized behavior.

Table 4: Comparison of dS/CFT toy model categories.

Feature	Analytic dS/CFT	Tensor-network dS/CFT	This work (causal graph)
Geometry	Fixed (black hole, hyperboloid)	Fixed (tiling)	Emergent (stochastic growth)
Tensors	N/A	Contracted	Conceptual only (not contracted)
Entanglement entropy	Analytic continuation / extremal surfaces	Minimal cut (RT)	Minimal cut (RT)
Numerical method	None	Single-instance quantum contraction	Ensemble classical graph cuts
Parameter tuning	Λ, mass, spin	Bond dimension χ	Ancestor probability p_{a}
Scaling law	Assumed linear	Derived or assumed	Measured, with error bars
Finite-size scaling	N/A	N/A	Explicitly verified

The entanglement slope is independent of the growth rate, demonstrating that the scaling is a topological property of the causal growth rule.

Linear scaling of minimal cuts is a hallmark of de Sitter holography. Our model therefore provides the first explicit, tunable, and numerically tractable causal graph realization of a dS/CFT toy model, with the ancestor probability controlling the effective cosmological constant.

By contrasting our construction with hyperbolic (AdS) tensor networks and with prior dS/CFT toy models, we highlight the essential ingredients—negative curvature and perfect tensors—required for criticality. Our work establishes a new class of holographic toy models—stochastic causal graphs—complementary to analytic gravitational and exact tensor-network approaches, and opens the door to statistical studies of holographic entanglement in de Sitter space.

Acknowledgements

The author thanks the anonymous reviewers for their constructive feedback, and acknowledges the open-source community for developing the software tools used in this work. This research did not receive any specific grant from funding agencies in the public, commercial, or not-for-profit sectors.

Code availability

All source code used to generate the data and figures in this paper is available at:

https://github.com/ComradeHB/causal-holographic-universe/tree/main

References

[1] J. M. Maldacena, "The Large-N Limit of Superconformal Field Theories and Supergravity," Adv. Theor. Math. Phys. **2**, 231 (1998) [arXiv:hep-th/9711200].

[2] F. Pastawski, B. Yoshida, D. Harlow, and J. Preskill, "Holographic quantum error-correcting codes: Toy models for the bulk/boundary correspondence," JHEP **06**, 149 (2015) [arXiv:1503.06237].

[3] G. Vidal, "Entanglement Renormalization," Phys. Rev. Lett. **99**, 220405 (2007) [arXiv:cond-mat/0512165].

[4] P. Calabrese and J. Cardy, "Entanglement entropy and conformal field theory," J. Phys. A **42**, 504005 (2009) [arXiv:0905.4013].

[5] S. Ryu and T. Takayanagi, "Holographic Derivation of Entanglement Entropy from AdS/CFT," Phys. Rev. Lett. **96**, 181602 (2006) [arXiv:hep-th/0603001].

[6] B. Swingle, "Entanglement Renormalization and Holography," Phys. Rev. D **86**, 065007 (2012) [arXiv:0905.1317].

[7] A. Strominger, "The dS/CFT Correspondence," JHEP **10**, 034 (2001) [arXiv:hep-th/0106113].

[8] E. Witten, "Quantum Gravity in De Sitter Space," [arXiv:hep-th/0106109].

[9] D. Anninos, "De Sitter Musings," Int. J. Mod. Phys. A **27**, 1230013 (2012) [arXiv:1205.3855].

[10] X. Dong, E. Silverstein, and G. Torroba, "De Sitter Holography and Entanglement Entropy," JHEP **07**, 050 (2018) [arXiv:1804.08623].

[11] M. Alishahiha, A. Karch, E. Silverstein, and D. Tong, "The dS/dS Correspondence," AIP Conf. Proc. **743**, 393 (2004) [arXiv:hep-th/0407125].

[12] D. Anninos, F. Denef, and D. Harlow, "Wave function of Vasiliev's universe: A few slices thereof," Phys. Rev. D **88**, 084049 (2013) [arXiv:1207.5517].

[13] V. Balasubramanian, J. de Boer, and D. Minic, "Mass, entropy and holography in asymptotically de Sitter spaces," Phys. Rev. D **65**, 123508 (2002) [arXiv:hep-th/0110108].

[14] G. W. Gibbons and S. W. Hawking, "Cosmological event horizons, thermodynamics, and particle creation," Phys. Rev. D **15**, 2738 (1977).

[15] A. Jahn, M. Gluza, F. Pastawski, and J. Eisert, "Holography and criticality in matchgate tensor networks," Sci. Adv. **5**, eaaw0092 (2019) [arXiv:1711.03109].

[16] B. Swingle, "Constructing holographic spacetimes using entanglement renormalization," [arXiv:1209.3304].

[17] D. Anninos, S. A. Hartnoll, and D. M. Hofman, "Static patch solipsism: Conformal field theory for the dS static patch," [arXiv:1209.3304].

[18] L. Susskind, "De Sitter Holography: Fluctuations, Anomalous Symmetry, and Wormholes," [arXiv:2106.03964].

[19] L. Niermann and T. J. Osborne, "Holographic networks for (1+1)-dimensional de Sitter spacetime," Phys. Rev. D **105**, 125009 (2022) [arXiv:2102.09223].

[20] C. Cao, W. Chemissany, A. Jahn, and Z. Zimborás, "Overlapping qubits from non-isometric maps and de Sitter tensor networks," JHEP (2023) [arXiv:2304.02673].